Broadband circulators based on directional coupling of one-way waveguides

Citation: Qiu, Wenjun, Zheng Wang, and Marin Soljačić. "Broadband Circulators Based on Directional Coupling of One-way Waveguides." Optics Express 19.22 (2011): 22248. © 2011 OSA

As Published: http://dx.doi.org/10.1364/OE.19.022248

Publisher: Optical Society of America

Persistent URL: http://hdl.handle.net/1721.1/76613

Version: Final published version: final published article, as it appeared in a journal, conference proceedings, or other formally published context

Broadband circulators based on directional coupling of one-way waveguides

Wenjun Qiu, Zheng Wang, and Marin Soljačić*

Department of Physics, Massachusetts Institute of Technology, 77 Massachusetts Avenue, Cambridge, Massachusetts 02139, USA

*soljacic@mit.edu

Abstract: Resonator-based optical circulators are fundamentally bandwidth-limited by their quality factors. We propose a new type of circulator based on directional coupling between one-way photonic chiral edge states and conventional two-way waveguides. The operational bandwidth of such circulators is tied to the bandwidth of the directional waveguide coupler and has the potential for simultaneous broadband operation and small device footprint.

OCIS codes: (230.5298) Photonic crystals; (230.3810) Magneto-optic systems.

References and links

1. R. J. Potton, "Reciprocity in optics," Rep. Prog. Phys. **67**(5), 717–754 (2004).
2. H. Takeda and S. John, "Compact optical one-way waveguide isolators for photonic-band-gap microchips," Phys. Rev. A **78**(2), 023804 (2008).
3. A. B. Khanikaev, A. V. Baryshev, M. Inoue, and Y. S. Kivshar, "One-way electromagnetic Tamm states in magnetophotonic structures," Appl. Phys. Lett. **95**(1), 011101 (2009).
4. A. B. Khanikaev, S. H. Mousavi, G. Shvets, and Y. S. Kivshar, "One-way extraordinary optical transmission and nonreciprocal spoof plasmons," Phys. Rev. Lett. **105**(12), 126804 (2010).
5. D. Jalas, A. Petrov, M. Krause, J. Hampe, and M. Eich, "Resonance splitting in gyrotropic ring resonators," Opt. Lett. **35**(20), 3438–3440 (2010).
6. J. Zheng, *Optical Frequency-modulated Continuous-wave (FMCW) Interferometry* (Springer, 2005).
7. M. Inoue, K. Arai, T. Fujii, and M. Abe, "Magneto-optical properties of one-dimensional photonic crystals composed of magnetic and dielectric layers," J. Appl. Phys. **83**(11), 6768–6770 (1998).
8. M. Levy, I. Ilic, R. Scarmozzino, R. Osgood, Jr., R. Wolfe, C. J. Gutierrez, and G. A. Prinz, "Thin-film-magnet magneto-optic waveguide isolator," IEEE Photonics Technol. Lett. **5**(2), 198–200 (1993).
9. Z. Wang and S. Fan, "Magneto-optical defects in two-dimensional photonic crystals," Appl. Phys. B **81**(2-3), 369–375 (2005).
10. Z. Wang and S. Fan, "Optical circulators in two-dimensional magneto-optical photonic crystals," Opt. Lett. **30**(15), 1989–1991 (2005).
11. Z. Wang and S. Fan, "Suppressing the effect of disorders using time-reversal symmetry breaking in magneto-optical photonic crystals: An illustration with a four-port circulator," Photonics Nanostruct. Fundam. Appl. **4**, 132–140 (2006).
12. W. Śmigaj, J. Romero-Vivas, B. Gralak, L. Magdenko, B. Dagens, and M. Vanwolleghem, "Magneto-optical circulator designed for operation in a uniform external magnetic field," Opt. Lett. **35**(4), 568–570 (2010).
13. K. Yayoi, K. Tobinaga, Y. Kaneko, A. V. Baryshev, and M. Inoue, "Optical waveguide circulators based on two-dimensional magneto photonic crystals: Numerical simulation for structure simplification and experimental verification," J. Appl. Phys. **109**, 07B750 (2011).
14. H. Zhu and C. Jiang, "Optical isolation based on Nonreciprocal Micro-Ring Resonator," J. Lightwave Technol. **29**(11), 1647–1651 (2011).
15. E. Ohm, "A Broad-Band Microwave Circulator," IRE Trans. Microwave Theor. Tech. **4**(4), 210–217 (1956).
16. J. Helszajn, *Nonreciprocal Microwave Junctions and Circulators* (Wiley, 1975).
17. M. Lohmeyer, M. Shamonin, and P. Hertel, "Integrated optical circulator based on radiatively coupled magneto-optic waveguides," Opt. Eng. **36**(3), 889 (1997).
18. N. Sugimoto, T. Shintaku, A. Tate, H. Terui, M. Shimokozono, E. Kubota, M. Ishii, and Y. Inoue, "Waveguide polarization-independent optical circulator," IEEE Photon. Technol. Lett. **11**(3), 355–357 (1999).
19. J. Fujita, "Hybrid-integrated optical isolators and circulators," in Proceedings Of SPIE (SPIE, 2002), Vol. 4652, pp. 77–85.
20. N. Hanashima, K. Hata, R. Mochida, T. Oikawa, T. Kineri, Y. Satoh, and S. Iwatsuka, "Hybrid Optical Circulator Using Garnet–Quartz Composite Embedded in Planar Waveguides," IEEE Photon. Technol. Lett. **16**(10), 2269–2271 (2004).
21. D. M. Pozar, "Ferrite Circulators," in *Microwave Engineering*, 3rd ed. (John Wiley & Sons, Inc., 2005), pp. 476–481.

#150213 - $15.00 USD Received 29 Jun 2011; revised 16 Aug 2011; accepted 4 Sep 2011; published 24 Oct 2011

22. F. D. Haldane and S. Raghu, "Possible realization of directional optical waveguides in photonic crystals with broken time-reversal symmetry," Phys. Rev. Lett. **100**(1), 013904 (2008).
23. Z. Wang, Y. D. Chong, J. D. Joannopoulos, and M. Soljacić, "Reflection-free one-way edge modes in a gyromagnetic photonic crystal," Phys. Rev. Lett. **100**(1), 013905 (2008).
24. Z. Yu, G. Veronis, Z. Wang, and S. Fan, "One-way electromagnetic waveguide formed at the interface between a plasmonic metal under a static magnetic field and a photonic crystal," Phys. Rev. Lett. **100**(2), 023902 (2008).
25. Z. Wang, Y. Chong, J. D. Joannopoulos, and M. Soljacić, "Observation of unidirectional backscattering-immune topological electromagnetic states," Nature **461**(7265), 772–775 (2009).
26. Q. Wang, Z. Ouyang, and Q. Liu, "Multiport photonic crystal circulators created by cascading magneto-optical cavities," J. Opt. Soc. Am. B **28**(4), 703 (2011).
27. K. Chiu and J. Quinn, "Magnetoplasma Surface Waves in Polar Semiconductors: Retardation Effects," Phys. Rev. Lett. **29**(9), 600–603 (1972).
28. R. Wallis, J. Brion, E. Burstein, and A. Hartstein, "Theory of surface polaritons in anisotropic dielectric media with application to surface magnetoplasmons in semiconductors," Phys. Rev. B **9**(8), 3424–3437 (1974).
29. Y. Poo, R. X. Wu, Z. Lin, Y. Yang, and C. T. Chan, "Experimental realization of self-guiding unidirectional electromagnetic edge states," Phys. Rev. Lett. **106**(9), 093903 (2011).
30. A. Yariv, "Coupled-mode theory for guided-wave optics," IEEE J. Quantum Electron. **9**(9), 919–933 (1973).
31. H. A. Haus, *Waves and Fields In Optoelectronics* (Prentice-Hall, 1984), Vol. 32.
32. I. Crassee, J. Levallois, A. L. Walter, M. Ostler, A. Bostwick, E. Rotenberg, T. Seyller, D. van der Marel, and A. B. Kuzmenko, "Giant Faraday rotation in single- and multilayer graphene," Nat. Phys. **7**(1), 48–51 (2011).
33. M. Jablan, H. Buljan, and M. Soljačić, "Plasmonics in graphene at infrared frequencies," Phys. Rev. B **80**(24), 245435 (2009).

1. Introduction

Nonreciprocal optical devices, such as circulators and isolators, are essential components in large-scale integrated photonic circuits, due to their ability to suppress crosstalk and fringes among constituent stages [1–5]. Circulators are widely used in fiber-optic interferometries to suppress laser noise and can be integrated with channel add/drop filters in switching applications [6]. In the past decade, the efforts to miniaturize nonreciprocal devices have been focusing on enhanced magneto-optical response in resonators and guided-wave structures [7,8]. Particularly, on-chip optical circulators have been proposed using photonic crystal resonators with overall dimensions at few-wavelength scale [9–16] and nonreciprocal waveguides at hundreds of wavelengths [17–20]. Resonator-based circulators rely on nonreciprocal coupling between waveguides and two counter-rotating resonant modes, where the resonant frequencies are split by magneto-optical effects [10,21]. As a consequence, resonant circulators are inherently narrow-band, with the operational bandwidth limited by the magneto-optical constants [10], irrespective of three-port or four-port configurations [9–11]. However, this inherent limit cannot be solved with very strong magneto-optical material alone, because reciprocal coupling directly occurs between the waveguides when they are closely placed to the resonator to lower quality factor.

To reconcile the needs for both large bandwidth and small device footprint, we propose to use recently-discovered one-way waveguides [22–25] to create broadband optical circulators with a device dimension on the order of tens of wavelengths. These photonic one-way modes are highly nonreciprocal: they propagate only along a single direction, while the backward modes are completely evanescent. In this paper, we use these fundamentally new states of light to create circulators that have the bandwidth potential to span an entire photonic bandgap. The circulators are based on directional couplers between a one-way edge waveguide and a conventional two-way waveguide. As a result, the operational bandwidth is determined by that of a waveguide coupler, without the inherent limit of a resonance. We employ both analytical spatial coupled mode theory and finite-element method to analyze such directional couplers and their performance as three-port circulators. A more complex four-port circulator will be also be presented, together with additional scattering matrix analysis, to elucidate the directions for further improvement in bandwidth.

2. Optical circulators based on one-way waveguides

Generally speaking, an optical circulator is a nonreciprocal multi-port device in which, under ideal conditions, light entering any given port is transmitted completely to the subsequent port. Reflected waves not only are blocked from entering upstream stages, but are also

#150213 - $15.00 USD Received 29 Jun 2011; revised 16 Aug 2011; accepted 4 Sep 2011; published 24 Oct 2011

separated and can be analyzed using additional optics. Optical circulators require a minimum of three ports, and more ports can be added by cascading multiple three-port circulators [16,26]. For this reason, we focus on the simplest three-port and four-port configurations in this paper.

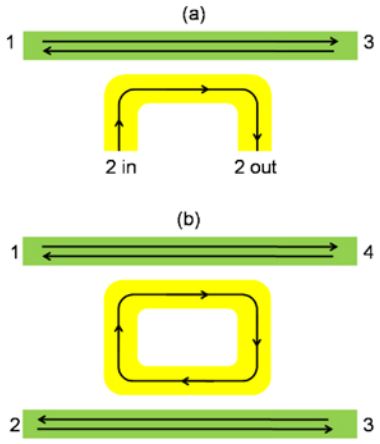

Fig. 1. Schematics of optical circulators based on one-way waveguides, with the port number illustrated. (a) A three-port circulator constructed from a directional coupler between a one-way waveguide (yellow) and a two-way waveguide (green). The arrows indicate the allowed propagation directions in each individual waveguide, in the absence of other waveguides. Coupling between adjacent waveguides alters the power flow and creates a circulator. (b) A four-port circulator created by cascading two three-port circulators.

Starting with a three-port circulator, we consider a one-way waveguide where light propagates in a single spatial mode along the forward direction, but is evanescent along the backward direction. A section of the one-way waveguide is placed in the vicinity of a two-way waveguide, in parallel, to form a waveguide coupler (Fig. 1a). Under a certain set of conditions which will be discussed in detail in the next section, complete energy transfer occurs for the forward modes between the two waveguides, and a three-port circulator is created. As illustrated in Fig. 1(a), the left and right ends of the two-way waveguide serve as Ports 1 and 3 respectively, while the input and output of Port 2 locate at the two ends of the one-way waveguide. Light entering Port 1 is completely transferred to the one-way waveguide through the directional waveguide coupler and is therefore transmitted to Port 2. In a similar fashion, light entering Port 2 is transmitted to Port 3. In contrast, the backward propagating mode remains in the two-way waveguide and consequently incident light to Port 3 travels to Port 1.

Cascading two three-port circulators produces a four-port circulator [16]. In our implementation, two three-port circulators described above are connected through port 2, resulting in a circulating one-way waveguide coupled to two two-way waveguides, as shown in Fig. 1(b). The ports reside at the ends of the two-way waveguides. Transmission from Port 1 to Port 2 and from Port 3 to Port 4 is mediated twice through waveguide couplers between sections of the one-way and the two-way waveguides. Transmission from Port 2 to Port 3 and from Port 4 to Port 1 takes place without interacting with the one-way waveguide. Overall, the system functions as a four-port circulator, with the ports distributed around the peripheral of the structure in an apparent counter-clock-wise direction opposite to the clock-wise circulation direction of the one-way waveguide.

At the heart of such waveguide-coupler-based circulators is a one-way waveguide where reflection is completely suppressed and full transmission occurs even at sharp corners or near large defects and scatterer. Two classes of one-way waveguides have been proposed: photonic chiral edge states [22,23,25] and surface magnetoplasmons [24,27,28]. Photonic chiral edge states flow at the truncated surfaces of a magneto-optical (gyromagnetic) photonic crystal in a particular frequency range where the bulk crystal features non-trivial topological properties.

#150213 - $15.00 USD Received 29 Jun 2011; revised 16 Aug 2011; accepted 4 Sep 2011; published 24 Oct 2011

In contrast, surface magnetoplasmons rely on the splitting and the directional-dependence of the surface plasmon frequency in the presence of a strong external magnetic bias [24]. Although both effects are purely two-dimensional, photonic chiral edge states have been experimentally realized in three-dimensional systems [25,29]. In this paper, we choose to focus on photonic chiral edge states, because of the additional degree of freedom from a large number of lattice choices, a large relative bandwidth, and low absorption loss in experimental systems [25]. Nevertheless the concept and the design principle can be readily transferred to surface magnetoplasmon systems.

3. Waveguide Coupler as a Three-Port Circulator

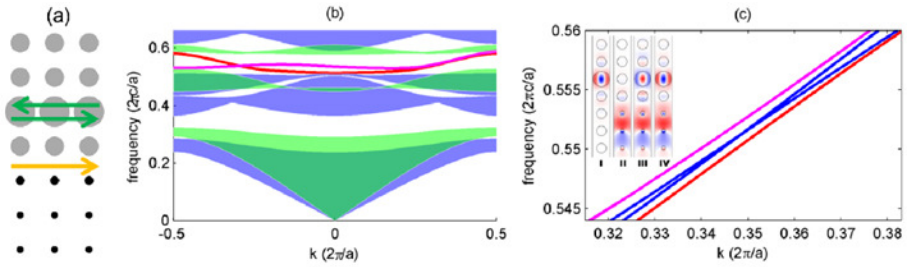

Fig. 2. Waveguide coupler between a photonic chiral edge state (one-way waveguide) and a two-way waveguide in a photonic crystal. (a) Schematics of the photonic crystal structure. The lower cladding is a gyromagnetic photonic crystal, while the upper cladding is a dielectric photonic crystal. (b) Calculated band diagram. The green and the blue regions are the projected band diagrams of the gyromagnetic photonic crystals and the dielectric photonic crystals respectively. An overlapping bandgap, $[0.527-0.576](2\pi c/a)$, supports a photonic chiral edge state (one-way) at the boundary between the two claddings. The top row of the lower cladding has enlarged rods to adjust the dispersion. The second lowest row of the upper cladding consists of enlarged rods to create a line-defect, serving as a two-way waveguide. The two waveguides couple strongly in the forward (left-to-right) direction. The eigenmodes of the coupled system are shown as the red and purple curves. (c) Dispersion relation in the *k*-space where the two forward modes are strongly coupled. The blue curves are unperturbed dispersion relations of the one-way and the two-way modes in the absence of coupling, where the mode profiles are shown in insets I and II. The red and purple curves are the dispersion relations of the compound modes in the presence of coupling (mode profiles shown in inset III and IV). The insets illustrate the calculated E-field distribution at $\omega = 0.551(2\pi c/a)$. For the entire frequency range shown, there is only one backward propagating mode as can be seen in panel (b).

A three-port circulator can be conveniently constructed from a waveguide coupler in two-dimensional photonic crystals. Taking a typical structure supporting photonic chiral edge state [23], where light travels only in one direction at the interface between a lower cladding of a gyromagnetic photonic crystal and an upper cladding of a nonmagnetic photonic crystal (Fig. 2a), we introduce an additional two-way waveguide by creating a line defect one lattice constant away from the interface.

The gyromagnetic photonic crystal consists of a square lattice of yttrium-iron-garnet (YIG) rods in air, with the rod radius $r_1 = 0.11a$ (a is the lattice constant). YIG exhibits strong gyromagnetic response under external magnetic bias, as the permeability tensor takes the form:

$$\mathbf{\mu} = \begin{bmatrix} \mu_{\parallel} & i\mu_{\perp} & 0 \\ -i\mu_{\perp} & \mu_{\parallel} & 0 \\ 0 & 0 & 1 \end{bmatrix} \qquad (1)$$

#150213 - $15.00 USD Received 29 Jun 2011; revised 16 Aug 2011; accepted 4 Sep 2011; published 24 Oct 2011

where $\mu_{\parallel} = 14$, $\mu_{\perp} = 12.4$, corresponding to conditions at 4.28GHz with an external magnetic field of 1600 Gauss [23]. The dielectric constant is $\varepsilon_1 = 15$. A bandgap supporting one-way chiral edge modes is found between $0.526 \times 2\pi c/a$ and $0.576 \times 2\pi c/a$ for the TM polarization (Fig. 2b) [23]. The dielectric constant and radius of the upper cladding ($\varepsilon_2 = 8$ and $r_2 = 0.285a$) are chosen to maximize the size of an TM bandgap (between $0.513 \times 2\pi c/a$ and $0.588 \times 2\pi c/a$)with the identical mid-gap frequency. At the interface between the two crystals, a one-way chiral edge state emerges through the entire frequency range where the two bandgaps overlap. We added the second waveguide by increasing the rod radius in the second lowest row of the upper cladding to 0.449*a* to introduce a line defect. This radius is chosen, together with an increase in the size of the rods in the top row of the lower cladding to 0.134*a*, the dispersion relations of the two waveguides intersect at a mid-gap frequency of $0.551 \times 2\pi c/a$ (Fig. 2c).

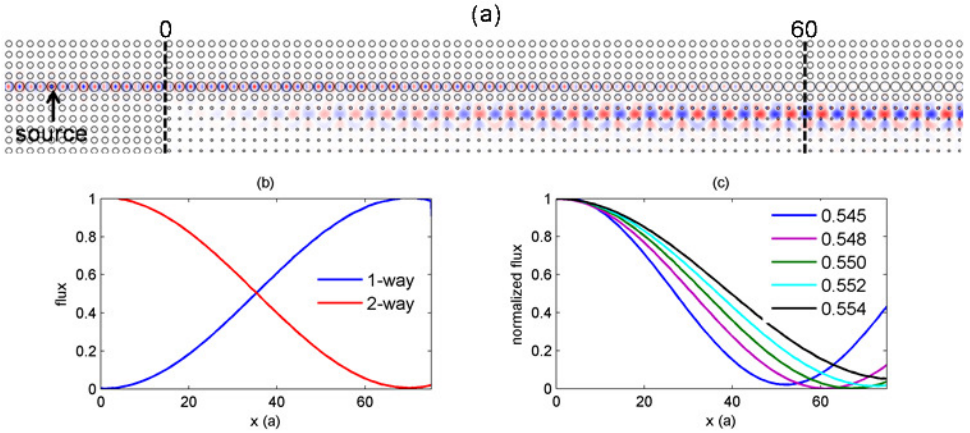

Fig. 3. Power transport in the waveguide coupler. (a) Steady state E-field pattern at $\omega = 0.551(2\pi c / a)$, showing a complete transfer from the two-way waveguide (incident from the left) to the one-way waveguide.(b) Light is transferred between the two-way waveguide and the one-way waveguide, as indicated by the power flux. (c) Power transfer over a range of frequencies.

The operational bandwidth of the waveguide coupler directly determines the bandwidth of the circulator. Therefore, it is important to review the analytical theory of a waveguide coupler that guides the design of the dispersion relation of the constituent waveguides. Such an analytical theory also points towards ways to improve transfer efficiency by controlling the difference in the phase velocity between the underlying waveguides. In the weakly-coupled regime, the amplitude of the waves in two parallel waveguides can be described by the following spatial coupled mode equations [30]:

$$\begin{cases} \dfrac{da_1}{dz} = -j\beta_1 a_1 + \kappa_{12} a_2 \\ \dfrac{da_2}{dz} = -j\beta_2 a_2 + \kappa_{21} a_1 \end{cases} \tag{2}$$

where a_i is the field amplitude and β_i is the wave vector in waveguide *i*, in the absence of the coupling. The coupling coefficients are related by energy conservation as $\kappa_{12} = -\kappa_{21}^*$, since the spatial coupled-mode theory is not restricted to reciprocal systems [30]. With the coupling

#150213 - $15.00 USD Received 29 Jun 2011; revised 16 Aug 2011; accepted 4 Sep 2011; published 24 Oct 2011

coefficient expressed in the absolute value $\kappa \equiv |\kappa_1| = |\kappa_2|$, the two eigenmodes in the coupled system possess different propagation constants

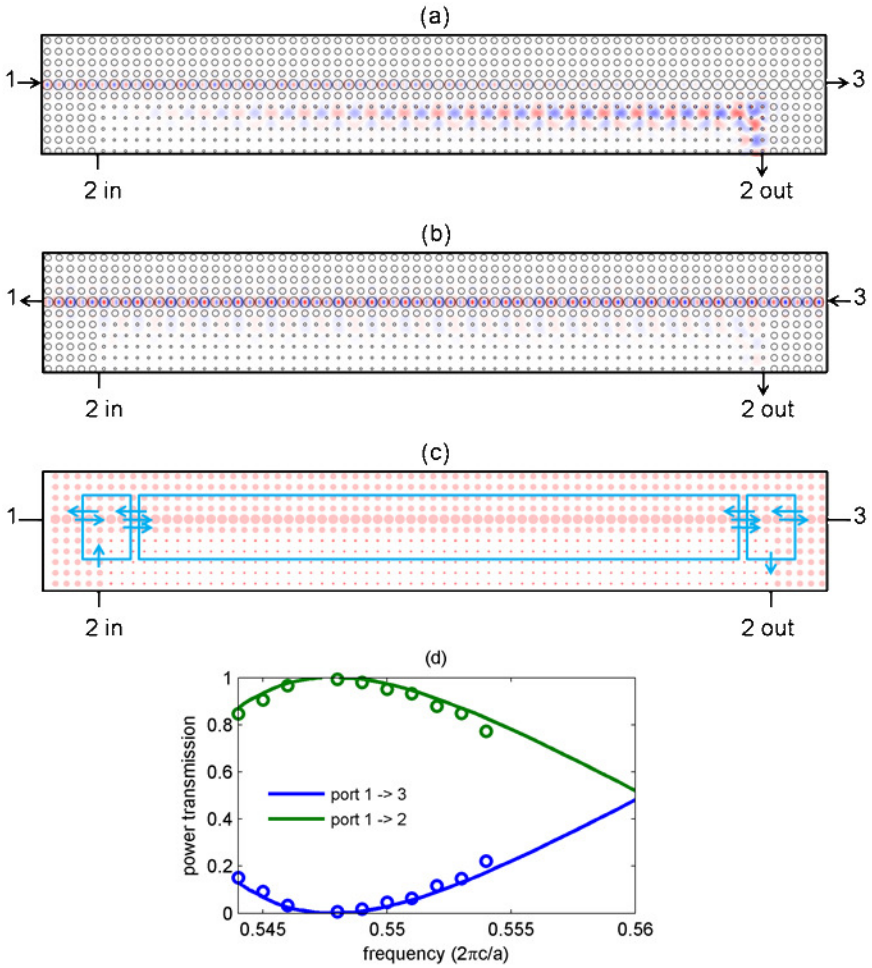

Fig. 4. Three-port circulator. (a) Steady-state electric-field distribution of a 3-port circulator excited from Port 1 at $\omega = 0.548(2\pi c / a)$. The waveguide coupler transfers light from the two-way waveguide to the one-way waveguide, producing complete transmission at Port 2. (b) Steady-state field distribution with excitation from Port 3 at $\omega = 0.548(2\pi c / a)$, where the transmission is routed to Port 1 instead. The leakage to Port 2 amounts to 0.5% of the total incident flux. (c) The scattering matrix decomposition of the three-port circulator. Arrows indicate distinct modes at boundaries. (d) The transmission spectra of the three-port circulator excited from Port 1.The finite element simulation (solid curves) agrees well with the scattering matrix calculation (circles).

$$k_{1,2} = \frac{\beta_1 + \beta_2}{2} \pm \sqrt{\left(\frac{\beta_1 - \beta_2}{2}\right)^2 + \kappa^2} \tag{3}$$

and their spatial field distributions are a linear combination of the individual waveguide modes (Fig. 2c). Light entering into either one of the constituent waveguide simultaneously excites both eigenmodes. Because of their different propagation constants, the spatial beating between the two transfers power between the two waveguides in a back-and-forth manner [31]. Maximum power transfer is given by

#150213 - $15.00 USD Received 29 Jun 2011; revised 16 Aug 2011; accepted 4 Sep 2011; published 24 Oct 2011

$$T = \frac{\kappa^2}{\left(\frac{\beta_1 - \beta_2}{2}\right)^2 + \kappa^2} \tag{4}$$

and reaches 100% when $|\beta_1 - \beta_2| \ll \kappa$. The interaction distance to achieve this maximal transfer is

$$L = \frac{\pi}{k_1 - k_2} = \frac{\pi}{2\sqrt{\left(\frac{\beta_1 - \beta_2}{2}\right)^2 + \kappa^2}} \tag{5}$$

The operation of an ideal circulator requires the waveguide coupler to satisfy the following two conditions over a broad range of frequencies: complete power transfer between the waveguides, and an identical interaction length. Consequently, for the constituent one-way waveguide and two-way waveguide, the ideal conditions include identical dispersion relation ($|\beta_1 - \beta_2| << \kappa$) and identical coupling constant κ over as broad frequency range as possible. In our design, the structure has been optimized such that both conditions are met over a relative bandwidth of ~2% (Fig. 2c).

The performance of the waveguide coupler is verified using a finite-element solver (Fig. 3a). A point source excites the two-way waveguide in the upper cladding, 11 lattice constants away from the convergence point where the one-way waveguide starts to run parallel to the two-way waveguide. Towards the right side of this convergence point, the waveguide coupler transfers power from the two-way waveguide to the one-way waveguide (Fig. 3b), as indicated by the flux in each waveguide as a function of the location. At the frequency of $0.551 \times 2\pi c/a$ where the uncoupled dispersion relations intersect, maximum power transfer reaches 100% efficiency, consistent with the coupled mode theory. Over the frequency range between $0.545 \times 2\pi c/a$ and $0.554 \times 2\pi c/a$, the peak transfer efficiencies hover above 95%, because $|\beta_1 - \beta_2| \ll \kappa$ is satisfied. A small variation in the coupling coefficient κ is observed in this range, resulting in a variation in the interaction length. Even though for a circulator one must use a fixed-length coupler for the entire operational bandwidth, we accomplished less than 1dB transmission ripple over a 2% relative bandwidth at a center frequency of $0.548 \times 2\pi c/a$ with a 60*a* long waveguide coupler.

Based on such a waveguide coupler, we can construct a three-port circulator as illustrated in Fig. 1a. At the center frequency of $0.548 \times 2\pi c / a$, complete transmission can be seen from Port 1 to Port 2 (Fig. 4a) and from Port 3 to Port 1 (Fig. 4b). The transmission spectra between these ports over a range of frequencies near the center frequency are shown in Fig. 4d. Even though the transmission from Port 1 to Port 2 decreases as the detuning from the center frequency increases, the sum of the transmission to Port 2 and Port 3 remains close to 1. The minimum reflection indicates the performance of the circulator is mainly limited by the bandwidth of the waveguide coupler, rather than the discontinuities in the system. Further structural optimization should yield more optimized dispersion relations for the constituent waveguides, given the large number of degrees of freedom in photonic crystal systems. The 1dB loss bandwidth for this circulator remains 2%.

We also performed scattering matrix analysis to isolate the impact of the waveguide coupler to the overall performance of the three-port circulator and the derived structures that will be discussed later in this paper. The three-port circulator is compartmentalized into three areas, two corner areas and a tri-mode area (a dual-mode waveguide coupler in the forward direction and a single-mode waveguide in the backward direction), as illustrated in Fig. 4c. Each area has three inputs and three outputs, corresponding to a 3x3 scattering matrix. In particular the tri-mode area is described by a simple diagonal matrix with a phase delay $e^{ik_i L}$

#150213 - $15.00 USD Received 29 Jun 2011; revised 16 Aug 2011; accepted 4 Sep 2011; published 24 Oct 2011

on the diagonal elements, where k_i is the propagation constant of the i-th eigenmode and can be conveniently calculated with mode solvers using plane-wave expansion or finite-element methods. The corner areas require three independent finite-element simulations to extract the matrix element of scattering matrix for each frequency. Combining the scattering matrices of all three areas, we obtain the total scattering matrix of the entire system, where: $|S_{21}|^2$ and $|S_{31}|^2$ are the transmission coefficients from Port 1 to Port 2 and from Port 1 to Port 3 respectively (Fig. 4d). A good agreement with the finite-element calculation of the full structures suggests that the scattering matrix analysis can be reliably used to examine performance of devices built from these constituent areas, such as cascaded three-port circulators in the next section.

4. Four-port circulator

As outlined earlier, additional ports can be introduced by cascading multiple three-port circulators. We present a specific example of synthesizing a four-port circulator by cascading two three-port circulators (Fig. 1b) by connecting the ports on the one-way waveguides. This implementation shares a single magneto-optical photonic crystal, on which a circulating edge mode is coupled to two parallel two-way waveguides subsequently and contains two directional couplers. At the previously calculated optimal frequency of the waveguide coupler at $0.548\times 2\pi c/a$, the four-port circulator also perform ideally in finite-element calculations: complete transmission occurs from Port 1 to Port 2 through the action of both waveguide couplers (Fig. 5a), while light incident on Port 4 is routed completely to Port 1 without interacting with the coupler(Fig. 5b). Similar transport behaviors are found between other ports as well.

At frequencies detuned from the optimal, the transmission of the four-port circulator is rather complex and we resort again to the scattering matrix formalism to understand the contributing factors. In so doing, we could efficiently compute the transmission spectra for devices with various lengths of the waveguide coupler and the vertical sections of the one-way waveguides. The four-port circulator can be decomposed into four corners and two horizontal tri-mode waveguides (coupler) and two vertical sections of a single-mode waveguide (one-way waveguide), as seen in Fig. 5c. Since we already know the scattering matrix of the corner and the dispersion relation of the waveguide coupler from previous analysis, the total scattering matrix of the four-port circulator can be calculated analytically by simple matrix calculations.

Since the waveguide coupler provides a bandwidth of around 2%, one might expect a similar drop in power transmission between the ports when the frequency is detuned from the optimal value. The calculated transmission spectrum (Fig. 5d) indeed exhibits a relative bandwidth of 1.3%, where the passband ripple is found to be less than 1dB. However, large transmission still occurs at a discrete set of frequencies far detuned from the optimal, even when the waveguide couplers do not provide complete power transfer. At these frequencies, residual power exists and circulates in the one-way waveguide, in contrast to the ideal case where residual power vanishes after propagating through both waveguide couplers (Fig. 5a). With the circulating residual power, the entire stretch of the one-way waveguide functions as a ring resonator, where complete transmission occurs when the phase accumulated through the entire one-way ring is an integer multiple of 2π. We verified this observation by changing the length of the vertical section of the one-way waveguides L_y and found the transmission peaks shift in frequency (Fig. 5f), commensurate with ring resonator interpretation. The notable exception is found at the optimal frequency of $0.548\times 2\pi c/a$, where the peak frequency is unaffected by L_y, consistent with a lack of residual power and the absence of the ring resonance. Further agreement is found in the simulation with a perfect absorber inserted in the left vertical section of the one-way waveguide: In that case, the circulating power is shut off completely, resulting in the disappearance of the oscillation.

#150213 - $15.00 USD Received 29 Jun 2011; revised 16 Aug 2011; accepted 4 Sep 2011; published 24 Oct 2011

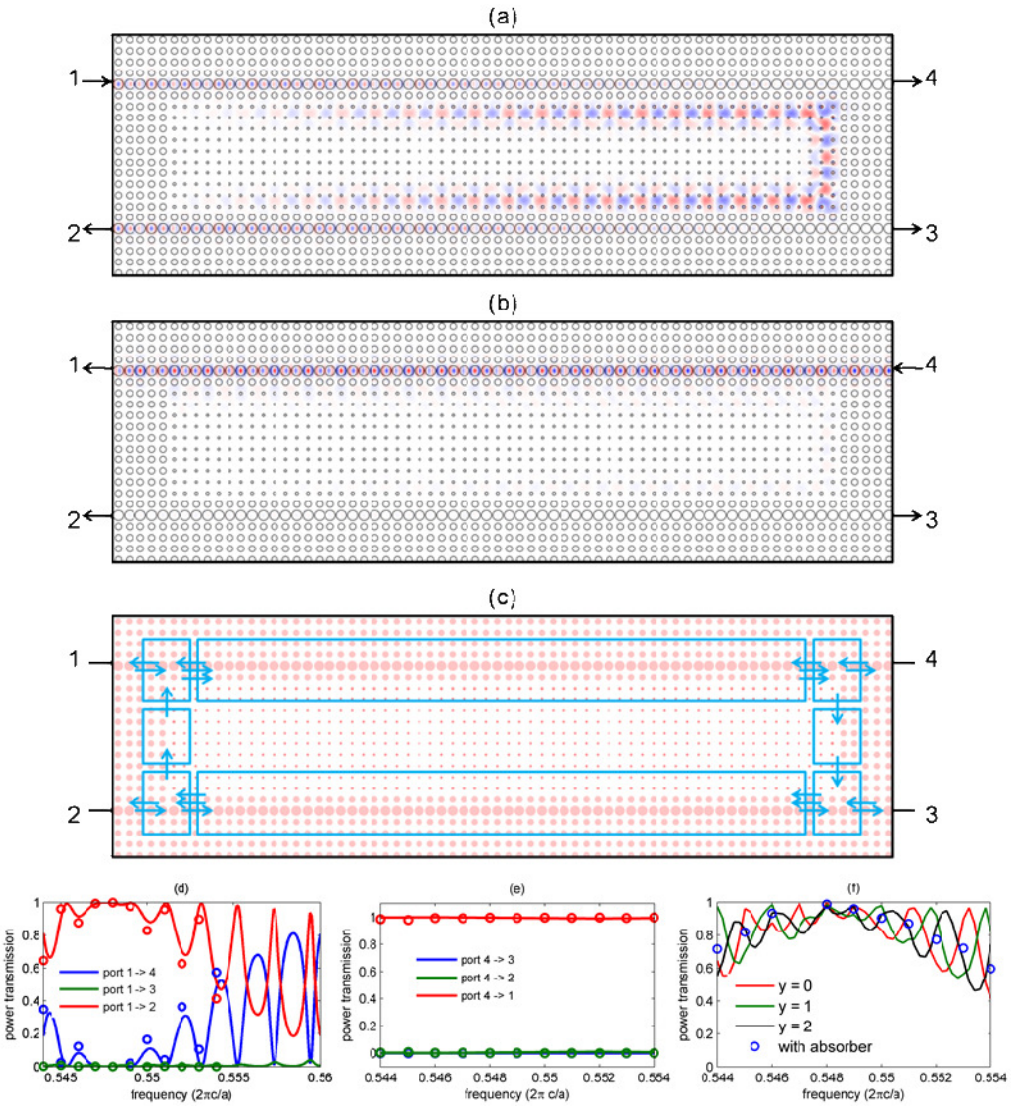

Fig. 5. Four-port circulator. (a) Steady-state electrical-field distribution of a four-port circulator excited from Port 1 at $\omega = 0.548(2\pi c / a)$, with full transmission to Port 2. (b) Steady-state field distribution with excitation from Port 4 at $\omega = 0.548(2\pi c / a)$. Full transmission is seen at Port 1. (c) Scattering matrix decomposition of the four-port circulator. (d, e) Transmission spectra of the four-port circulator. Finite element simulation (curves) shows good agreement with scattering matrix calculation (circles). The input is at port 1 in (d) and port 4 in (e). (f) Finite-element-simulated transmission spectra for three circulators with various lengths for the vertical sections of the one-way waveguide (curves). The finite-element-simulated transmission spectrum with an absorber is inserted in the one-way waveguide between Port 1 and Port 2 (circles).

We note that such waveguide-coupler based circulators, in both three-port and four-port forms, can eventually provide much greater bandwidth, when one optimizes the dispersion relation of the underlying one-way and two-way waveguides. Here both the geometry of the photonic crystals and the frequency-dependent gyromagnetic tensor elements affect the dispersion. The incomplete transmission at detuned frequencies could originate from the reflection from the 90° bend or a non-ideal waveguide coupling. However, since the

#150213 - $15.00 USD Received 29 Jun 2011; revised 16 Aug 2011; accepted 4 Sep 2011; published 24 Oct 2011

aggregated transmission to Port 2 for the three-port circulator (Fig. 4d) and the aggregated transmission to Port 2 for the four-port circulator (Fig. 5d) are both close to unity, the performance limitation is largely dominated by the waveguide coupler. There is also a trade-off between the bandwidth and the length of the waveguide coupler in this proof-of-concept structure. However, given the large degree of freedom in dispersion engineering for photonic crystals, by varying the dimension and the shape of the nearest unit cells to the waveguides, one could in principle match the uncoupled dispersion relations of the two waveguides, over a much broader range of the frequency. In other words, equalizing the propagation constant and the frequency of the two waveguides could allow us to create ideal circulators over a frequency range close to the entire photonic bandgap. Moreover, increasing the coupling coefficient κ by physically merging the two-way waveguide and the one-way waveguide could reduce the interaction length, thereby reducing the overall device dimension significantly. With the emergence of novel infrared magneto-optical materials featuring the Voigt parameter comparable to microwave ferrites [32,33] envision the experimental demonstration of such broadband circulator at optical frequencies.

5. Concluding Remarks

In this paper, we proposed a novel optical circulator based on directional couplers between a one-way waveguide and a two-way waveguide. We examined the bandwidth limit of such a waveguide coupler and its impact on the derived three-port circulators and four-port circulators. The bandwidth is not limited by the resonant linewidth and a three-port circulator and a four-port circulator are implemented numerically to feature a relative 1dB -bandwidth of 2% and 1.3% respectively. While our discussion has been restricted to two-dimensional structures, the operational principle and design procedures can be readily extended to three-dimensional structures at microwave, THz and optical frequencies, using out-of-plane confinement employed in experimental three-dimensional chiral edge state systems [25].

Acknowledgements

This work was supported in part by the MRSEC Program of the National Science Foundation under award number DMR-0819762, and in part by the Army Research Office through the Institute for Soldier Nanotechnologies under Contract No. W911NF-07-D0004.

#150213 - $15.00 USD Received 29 Jun 2011; revised 16 Aug 2011; accepted 4 Sep 2011; published 24 Oct 2011